Capture Cross Sections and Radiative Emission-Line Strengths for Slow Ne^{8+} Collisions with He and H_2

Anthony C. K. Leung * and Tom Kirchner *

Department of Physics and Astronomy, York University, Toronto, ON M3J 1P3, Canada
* Correspondence: leungant@yorku.ca (A.C.K.L.); tomk@yorku.ca (T.K.)

Abstract: The Ne^{8+}–He and –H_2 collision systems are examined at impact speeds ranging between 0.17 and 0.4 a.u. Transition probabilities for electron capture are obtained using the two-center basis generator method performed within the independent-electron model. The aim of calculating capture cross sections for these collision systems is to provide new theoretical verification of previously reported experimental data and to provide aid for astrophysical X-ray studies. This study also examines the applicability of the independent-electron model with effective potentials to describe two-electron capture for these two systems. Comparisons of capture cross sections and radiative-emission counts with the available experimental and theoretical data show an overall good agreement.

Keywords: ion–atom collisions; ion–molecule collisions; post-collisional de-excitation processes

1. Introduction

Obtaining accurate state-selective cross sections from slow charge-exchange collisions has become a focus in recent times because of the importance of such data in studies of astrophysical plasma environments [1–3]. From the perspective of astrophysical applications, *nl* partial capture cross sections are used in solar-wind charge-exchange models to study, for example, the X-ray flux in the heliosphere [4–6] and radiation from the outer rims of supernova remnants [7,8]. Technological advances and the development of new experimental and theoretical techniques allow one to explore collision systems relevant to these astrophysical problems in greater detail [9–12].

In this work, the interest is in slow Ne^{8+} collisions with He and H_2 and the subsequent radiative emissions due to single-electron capture (SEC). Because autoionizing double-capture (ADC) can also contribute to the overall SEC cross sections, this process is also examined in this work. Several groups have reported experimental cross sections [13–15] and radiative-emission spectra [16] several decades ago, but the large uncertainties in the measurements can make comparisons inconclusive [17]. This also applies to comparisons of *nl* cross sections [18], since accurate theoretical data are scarce. A modern approach to highly resolved X-ray measurements in merged-beam experiments involves the use of a microcalorimeter detector [19]. Such a detector is capable of resolving X-ray signals of no more than 10 eV full-width at half-maximum [19]. Recent reports on measurements of radiative emissions from Ne^{8+}–He collisions using the X-ray microcalorimeter detector [20,21], motivate the further theoretical examination of these systems.

Theoretical approaches, such as the coupled-channel method performed within an independent-electron model (IEM) [22], are very capable of describing SEC in slow collisions with He [23–25]. Chen and Lin [26] used a variant of the independent-electron description in the single-particle Hamiltonian and showed that it can adequately describe the features of double-electron capture (DEC) in Ne^{8+}–He collisions. Theoretical studies of Ne^{8+}–H_2 collisions are scarce, but it has been shown that an effective model potential treatment of H_2 in IEM collision calculations [27] is

suitable for describing SEC and DEC without resorting to ab initio methods so long as the collision is fast enough that vibrational and rotational effects can be safely neglected. For this reason, the present analysis also aims to show that such an approach is applicable to the Ne^{8+}–H_2 system.

In this article, a theoretical analysis of slow Ne^{8+}–He and –H_2 collisions with new capture cross sections based on the IEM framework and the use of effective potentials is presented. The nonperturbative, coupled-channel two-center basis generator method (TC-BGM) [28] was employed to obtain single-particle capture probabilities. The main feature of the TC-BGM is that it allows calculations to reach convergence without resorting to a large basis set. The IEM TC-BGM has been applied to study electronic processes in various systems [29–32], including problems related to collision-induced radiative emissions [33–36]. A summary of this theoretical framework and the approach to post-collision analyses is provided in Section 2. In Section 3, the calculated capture cross sections are assessed in two ways vis-à-vis the available data: (i) directly comparing with absolute cross sections, and (ii) indirectly by means of comparing radiative-emission counts produced by these charge-exchange collisions. It should be noted that atomic units ($\hbar = e = m_e = 4\pi\epsilon_0 = 1$) are used throughout the article unless stated otherwise.

2. Theoretical Approach

The focus of this work is on collision-induced radiative emissions at impact speeds ranging between 0.17 and 0.4 a.u. (i.e., 0.7 and 4 keV/amu). The theoretical framework for this study is similar to the IEM analysis of the C^{6+}–He and –H_2 collisions in Reference [35]. For this reason, only a summary highlighting the core details and the model potential treatment is given.

For the collision calculation, the semiclassical approximation was employed by assuming the target is fixed in space and the Ne^{8+} projectile travels in a straight-line path at constant speed v_P, described by $\mathbf{R}(t) = (b, 0, v_P t)$, where b is the impact parameter. Within the IEM description, the goal is to solve a set of single-particle time-dependent Schrödinger equations,

$$i\frac{\partial}{\partial t}\psi_i(\mathbf{r}, t) = \hat{h}(t)\psi_i(\mathbf{r}, t), \ i = 1, ..., N, \tag{1}$$

for the initially occupied orbitals on the target. By assuming that the strongly bound K-shell electrons in the Ne^{8+} ions remain frozen during the collision, the single-particle Hamiltonian can be decomposed as

$$\hat{h}(t) = -\frac{1}{2}\nabla^2 + V_P(|\mathbf{r}_P|) + V_T(|\mathbf{r}|, t), \tag{2}$$

where $\mathbf{r}_P$ is the electron position vector with respect to the projectile and is related to that with respect to the target by $\mathbf{r}_P(t) = \mathbf{r} - \mathbf{R}(t)$. In this work, $V_P = V_{Ne^{8+}}$ is represented by the model potential [37][1],

$$V_{Ne^{8+}}(r_P) = -\frac{8}{r_P} - \frac{2}{r_P}\left(1 + \frac{\alpha}{2}r_P\right)e^{-\alpha r_P}, \tag{3}$$

with $\alpha = 18.037$. As for the target potentials, starting with the He target, an effective ground-state potential which includes exact exchange from calculations using the optimized potential method of density functional theory [38] is used. The H_2 target is represented by an effective single-center, spherical model potential [27]

$$V_{H_2}(r) = -\frac{1}{r} - \frac{1}{r}(1 + \alpha r)e^{-2\alpha r}, \tag{4}$$

with $\alpha = 3.93$. Furthermore, another variant of the target potential is considered where a time-dependent screening potential [39] due to electron removal during the collision is included.

---

[1]   There is a minor typo in Equation (A27) of Reference [37]; the potential expression should be $V(r) = -(Z - n_c)/r + \Omega(r)$, where $\Omega(r)$ is the second term of Equation (3) above, such that the asymptotic behavior $V(r) \rightarrow -Z/r$ as $r \rightarrow 0$ is satisfied.

To distinguish the results from these two variants in this work, those which use this screening model are referred to as *target-response* (or simply *response*), while those in which the ground-state potentials are frozen are referred to as *no-response* approximation. It has been shown in previous investigations [35,39,40] that the use of such a time-dependent screening model typically leads to improved agreement with experimental total cross sections in the low- to intermediate-energy regime. For applications on state-selective capture, the use of such a screening model can have mixed effects on the radiative-emission results [35,36]. For these reasons, the main purpose of performing calculations with these two potential variants is to gain insight into the range of results that can be produced by the present theory and to gauge the 'uncertainty' of the present method [41].

The set of single-particle equations is solved by projecting them onto a finite set of basis states and propagating them using the TC-BGM. Here, the basis sets include: all nlm states from $n = 2$ to $n = 7$ of the Ne^{7+} projectile, all states from the *KLMN* shells of the target, and a set of BGM pseudostates [28] to account for quasimolecular couplings and transitions to the continuum. Once the single-particle capture probabilities p^{cap} are obtained, they are combined statistically by using a multinomial analysis which describes q-fold capture with simultaneous k-fold ionization P^{qk} [42,43]. For the present study, *pure* SEC is

$$P^{10} = 2p^{cap}(1 - p^{cap} - p^{ion}),\qquad(5)$$

while DEC is

$$P^{20} = (p^{cap})^2.\qquad(6)$$

In practice, these calculations are performed on the level of nl-states to be used for the post-collision analysis. With these probabilities, the corresponding cross sections σ_{cap} can be obtained by integrating over the impact parameter plane,

$$\sigma_{cap} = 2\pi \int_0^\infty b P^{q0}(b)db.\qquad(7)$$

For the post-collision analysis of Auger and radiative transitions on the projectile, it is sufficient to solve the standard rate equations [44,45] subject to the initial capture populations represented by σ_{nl} cross sections. Specifically, the population N of some energy level p is governed by

$$\frac{dN_p(t)}{dt} = \sum_{i=p+1}^m N_i(t)A_{i\to p} - N_p(t)\sum_{f=1}^{p-1} A_{p\to f},\qquad(8)$$

where A is a transition rate. Note that the population level index is a multi-index in practice, and transitions can occur through intermediate states dictated by selection rules. Accurate transition rates are obtained by the RATIP program [46] which provides ab initio calculations of the electronic structure and properties of atoms and ions. To be consistent with the IEM, calculations using the RATIP program are restricted to single configurations and assume that the two-electron states are singlet states, since spin changes from the singlet He and H_2 ground states are unlikely [47].

Total photon counts for specific transitions are then obtained by integrating the intensity expression [45]

$$(\text{counts})_{nl\to n'l'} = A^{rad}_{nl\to n'l'} \int_0^\infty N_{nl}(t)dt.\qquad(9)$$

Since the dominant capture channel is $n = 4$ and $n = 5$ for collisions with He and H_2, respectively, only radiative transitions corresponding to cascades of $n = 3, 4,$ and 5 are considered.

3. Results and Discussion

3.1. Capture Cross Sections

Figure 1 shows the total capture cross sections for Ne^{8+} collisions with He (Figure 1a) and H_2 (Figure 1b). In each plot, results of pure SEC are shown separately from total SEC (i.e., pure SEC +

ADC). The present TC-BGM results are compared with total SEC measurements after post-collision ADCs [48,49], spectroscopy measurements [13,14], and coupled-channel calculations using one-electron diatomic orbitals (OEDM) [17]. Note that ADC mainly contributes to the production of the $Ne^{7+}(1s^2 2p)$ state for these collisions [17,50]. Since the reported cross sections only included capture contributions from the $n = 3$ and $n = 4$ states, it is justified to treat those values as pure SEC.
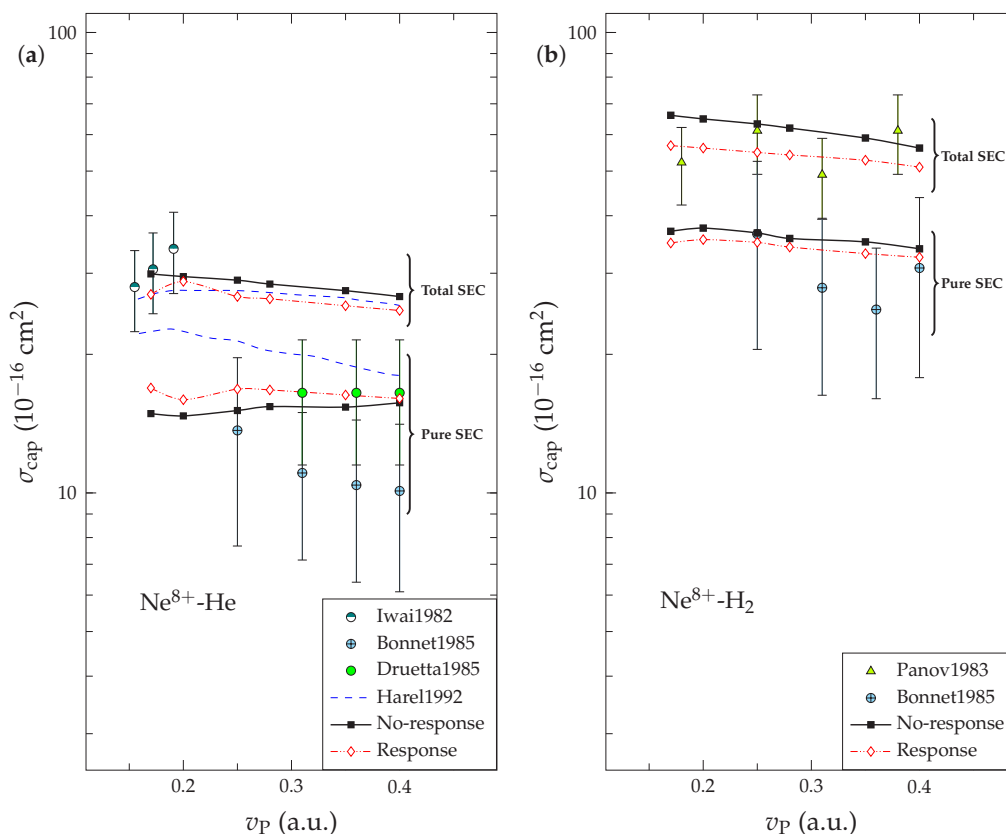

Figure 1. (**a**) Total capture cross sections with respect to the impact speed for Ne^{8+}–He collisions. Pure single-electron capture (SEC) cross sections are separated from total SEC (pure SEC + autoionizing double-capture (ADC)). Experiments: Iwai et al. [48], Bonnet et al. [13], Druetta et al. [14]. Theory: Harel and Jouin [17], present work (no-response approximation and target-response model). (**b**) Same as (**a**) but for Ne^{8+}–H_2 collisions. Experiments: Panov et al. [49], Bonnet et al. [13]. Theory: present work.

By examining the SEC cross sections for both collision systems, it can be seen that the present results are within the experimental uncertainties. For the Ne^{8+}–He system, the present total SEC also agrees very well with the OEDM calculations regardless of the different variants in the target potential that were used in the present calculations since they appear similar in magnitude. A similar agreement is also shown for the pure SEC cross sections at $v_P = 0.4$ a.u., but the deviation between the two calculations grows as impact speed decreases. One can then conclude that the pure SEC and ADC cross section ratios are different. Furthermore, comparing the cross sections between the two collision systems shows that those corresponding to the H_2 target are larger. This can be understood by the fact that the primary capture state for H_2 collisions is higher than that for He collisions. As a result, capture is extended over a larger spatial region, which then leads to a larger total cross section.

In a previous TC-BGM analysis of slow C^{6+}–He collisions [35], it was found that ADC cross sections for C^{6+}–He collisions were grossly overestimated when the IEM was employed and that the so-called *independent-event model* [51] is more appropriate for that system. We note that the coupled-channel calculation of Chen and Lin [26] for capture in the Ne^{8+}–He system to individual doubly excited states is similar in spirit to the independent-event model [51]. From Figure 1, it is

evident that the present IEM description is sufficient to describe *total* ADC for both He and H_2 collisions with the more highly charged Ne^{8+} projectiles. All of these theoretical remarks are consistent with the results of the differential cross section studies by Boudjema et al. [50] and Roncin et al. [52], where total DEC (or ADC) for the He target appears at least as probable as total SEC for collisions which involve projectile ions with charge $q \geq 7$ (or $q \geq 6$ for H_2). Furthermore, Boudjema et al. [50] also noted that the ADC to pure SEC ratio decreases at lower impact speeds [53]. This behavior is shown in Figure 1a for the OEDM calculations but not in the present work.

To further assess the total ADC cross sections, a few values at $v_P = 0.4$ a.u. are listed in Table 1 from the present calculations and earlier works. There is reasonable agreement between all independent studies for both collision systems at this impact speed. Based on the curves in Figure 1 and the discussion above regarding the ADC to pure SEC ratio behavior, it is implied that the present ADC may be slightly overestimated compared with the OEDM results [17] at lower impact speeds. As discussed in the next subsection for Ne^{8+}–H_2 collisions, such an overestimation of ADC can impact the radiative-emission results.

Table 1. Total ADC cross sections (in 10^{-16} cm^2) for Ne^{8+}–He and Ne^{8+}-H_2 collisions at $v_P = 0.4$ a.u. Theory: present independent-electron model (IEM) two-center basis generator method (TC-BGM) in the no-response and response models; Harel and Jouin [17]. Experiment: Mack [54] (25% uncertainty); Bordenave-Montesquieu et al. [55] (35% uncertainty).

$v_P = 0.4$ a.u.	σ_{ADC}	
	Ne^{8+}–He	Ne^{8+}–H_2
No-response	10.8	24.1
Response	9.6	19.3
Ref. [17]	≈ 7	
Ref. [54]	10	25.6
Ref. [55]	17	36

Figure 2 compares the present $4l$ capture cross sections for He collisions (Figure 2a) and $5l$ cross sections for H_2 collisions (Figure 2b) with previous spectroscopic measurements by Bonnet et al. [13], Druetta et al. [14], and Beijers et al. [15]. For this comparison, the focus is on pure SEC into the main capture channels. Contrary to the findings of Bonnet et al. [13], who concluded that capture in H_2 collisions is distributed over the $n = 4$ and $n = 5$ states, the present results only show selective capture in $n = 5$.

Qualitatively, the present cross sections for both systems show typical behavior with respect to the impact speed. Specifically, capture to high l-states is preferable in faster collisions due to stronger rotational coupling, while preference to low l-states is shown for slower collisions due to stronger radial coupling [56]. The cross sections for the highest l-states (i.e., $4f$ and $5g$ for He and H_2, respectively) appear to contradict this trend; however, the behavior of increasing capture into those states is expected to occur in much faster collisions [37]. The only set of experimental data that appears to be consistent with this behavior is that reported by Bonnet et al. [13]. Those from other groups are inconclusive due to a lack of data over the range of impact speeds of interest.

Overall, the present results are in reasonable agreement with the experimental cross sections. The only set of data that deviates remarkably in some instances is that of Beijers et al. [15]. It can be seen that many of those cross sections appear large[2]. Specific cases, such as σ_{4p} in He collisions (Figure 2a), show a large discrepancy between the results of Bonnet et al. [13] and Druetta et al. [14]. Here, the present results appear closer to the former. There is also a wide discrepancy between the two

---

[2]   When the σ_{4l} cross sections of Beijers et al. [15] are added, the sum is similar in magnitude to the total SEC shown in Figure 1a, which conflicts with the pure SEC cross sections from other experimental and theoretical results. For this reason, total cross sections of Beijers et al. [15] are not shown in Figure 1a in order to avoid confusion.

measurements for σ_{4f}, in which case the present results are closer to those of Druetta et al. [14]. In other words, the present results do not necessarily match with one specific experiment. Another exceptional case is σ_{5f} in H_2 collisions (Figure 2b), where the present results are much larger than those of Bonnet et al. [13]. This partially explains the differences in the total cross sections shown in Figure 1. The cause of these discrepancies can be partially attributed to systematic experimental errors related to the anisotropy of measured emissions, which can affect the branching ratios of cascades [13].
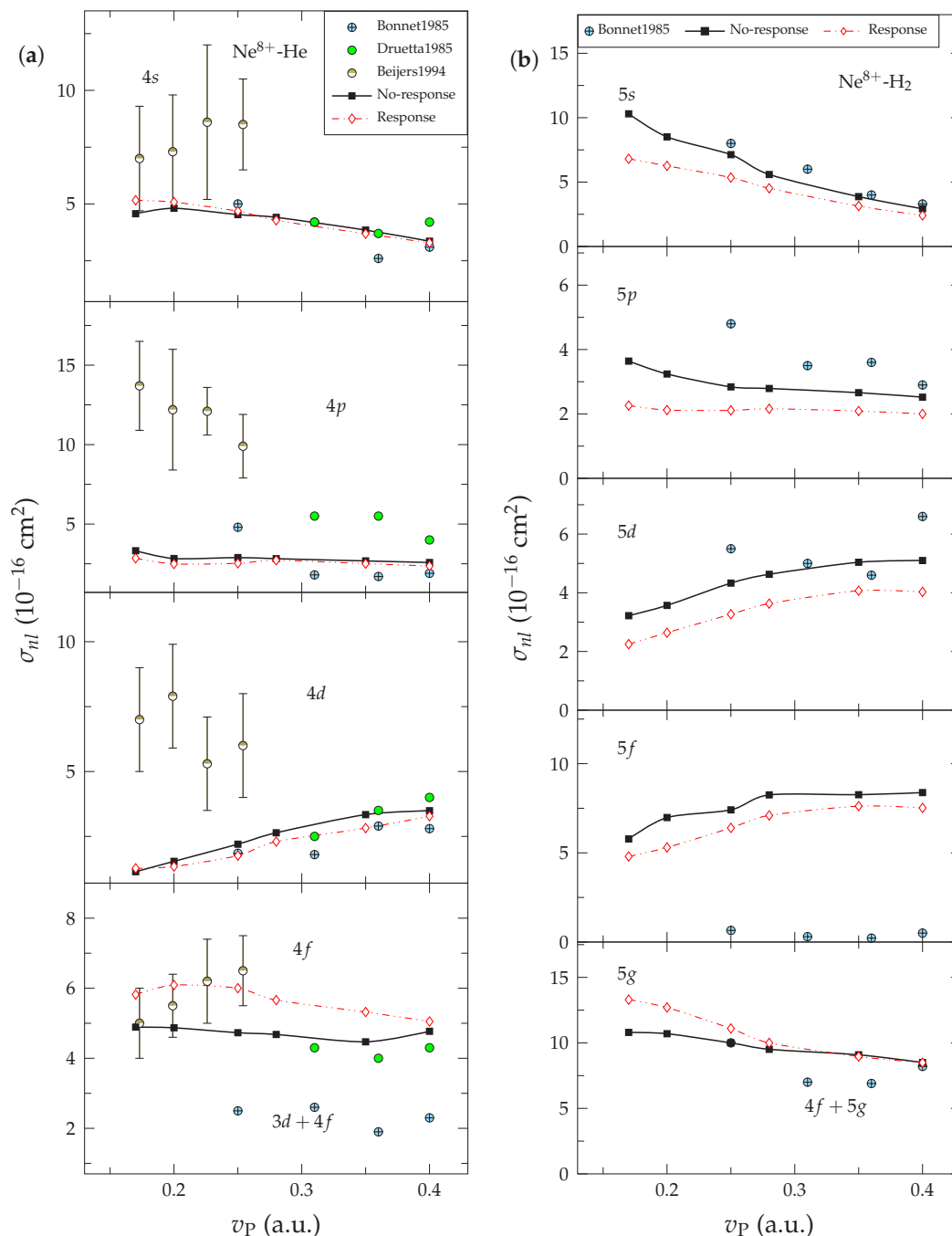
Figure 2. (**a**) Partial capture cross sections of $4l$-states with respect to the impact speed for Ne^{8+}–He collisions. Capture events correspond to pure SEC only. Experiment: Bonnet et al. [13] (40% uncertainty); Druetta et al. [14] (30% uncertainty); Beijers et al. [15]. Theory: present work (no-response approximation and target-response model). (**b**) Same as (**a**) but $5l$-states for Ne^{8+}–H_2 collisions.

3.2. Line-Emission Results

Radiative-emission counts with respect to impact speed from charge-exchange Ne^{8+}–He collisions are shown in Figure 3. These emission counts are normalized with respect to the total counts for the transitions that are shown in the figure. Recall that the focus is on line emissions from cascades in $n = 3$ and $n = 4$ states for this system. Also recall from the above discussion that such cascades are the result of pure SEC only. The present calculations are compared with spectroscopic measurements by Fleury et al. [16] and measurements using a high-resolution X-ray quantum microcalorimeter [20,21].
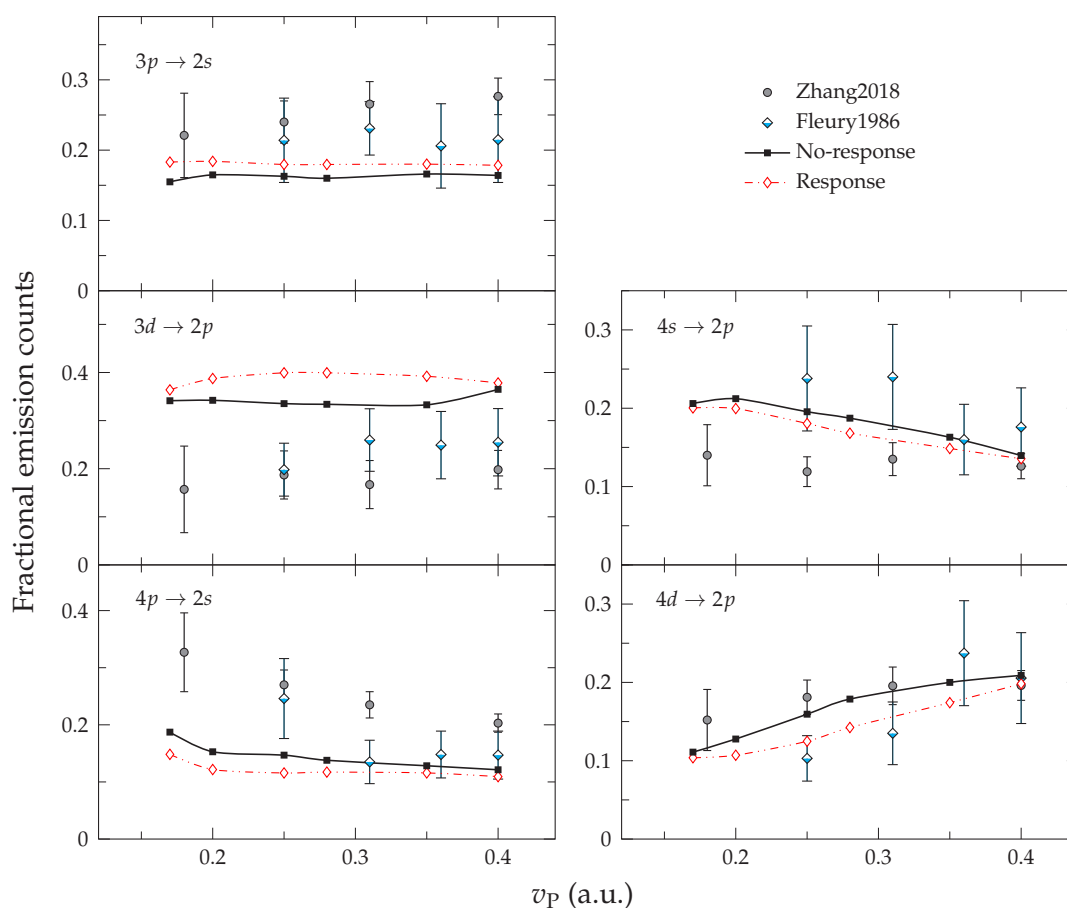

Figure 3. Fractions of line emissions with respect to impact speed from charge-exchange Ne^{8+}–He collisions. Experiments: Zhang et al. [20,21]; Fleury et al. [16]. Theory: present work.

The line-emission results produced by the two TC-BGM variants of no-response vs. the target-response model appear similar to each other, with a quantitative difference of 25% or less. Overall, the line-emission profiles from the present calculations are qualitatively similar to the experimental counts. Quantitatively, the present results appear to be closer to the results of Fleury et al. [16] than to those of Zhang et al. [20,21]. Moreover, specific transition counts, such as $3d \to 2p$, appear slightly overestimated compared with both experiments, which suggests a large σ_{4f} in the present calculation (cf. Figure 2a). For the $4p \to 2s$ transition, noticeable deviations from the measurements are found at low impact speeds, which is a result of a smaller σ_{4p} from the present calculations.

In a similar fashion, Figure 4 shows the fractional emission counts with respect to impact speed for Ne^{8+}–H_2 collisions. For this comparison, only measurements by Fleury et al. [16] are available to benchmark the present results. Because the main capture channel is a higher-energy state $n = 5$ compared with $n = 4$ for He collisions, additional transitions can be observed for this system. In addition, since ADC can have a sizable contribution to $Ne^{7+}(1s^23l)$ production due to decay

from certain $Ne^{6+}(1s^24ln'l')$ states [54], additional results of the present calculations which include ADC are shown as well. It should be noted that Fleury et al. [16] did not discuss the role of ADC in their measurements, and thus, it is not clear whether these results do include ADC. Using the work of Boudjema et al. [50] as an experimental guidance on the double-capture mechanism for the Ne^{8+}–H_2 system, only Auger decay from $4l5l'$ states are included in the $3l$ cascades in the present calculations. Contrary to the good agreement between the experimental total SEC data shown in Figure 1b and the present calculations which include ADC from all possible doubly-excited states, it should be noted that the IEM does not necessarily produce the correct proportions of *state-selective* double-capture. As an example, the present calculation shows that the production of $Ne^{6+}(5l5l')$ for H_2 collisions is the largest, which is in disagreement with the experimental value [50].

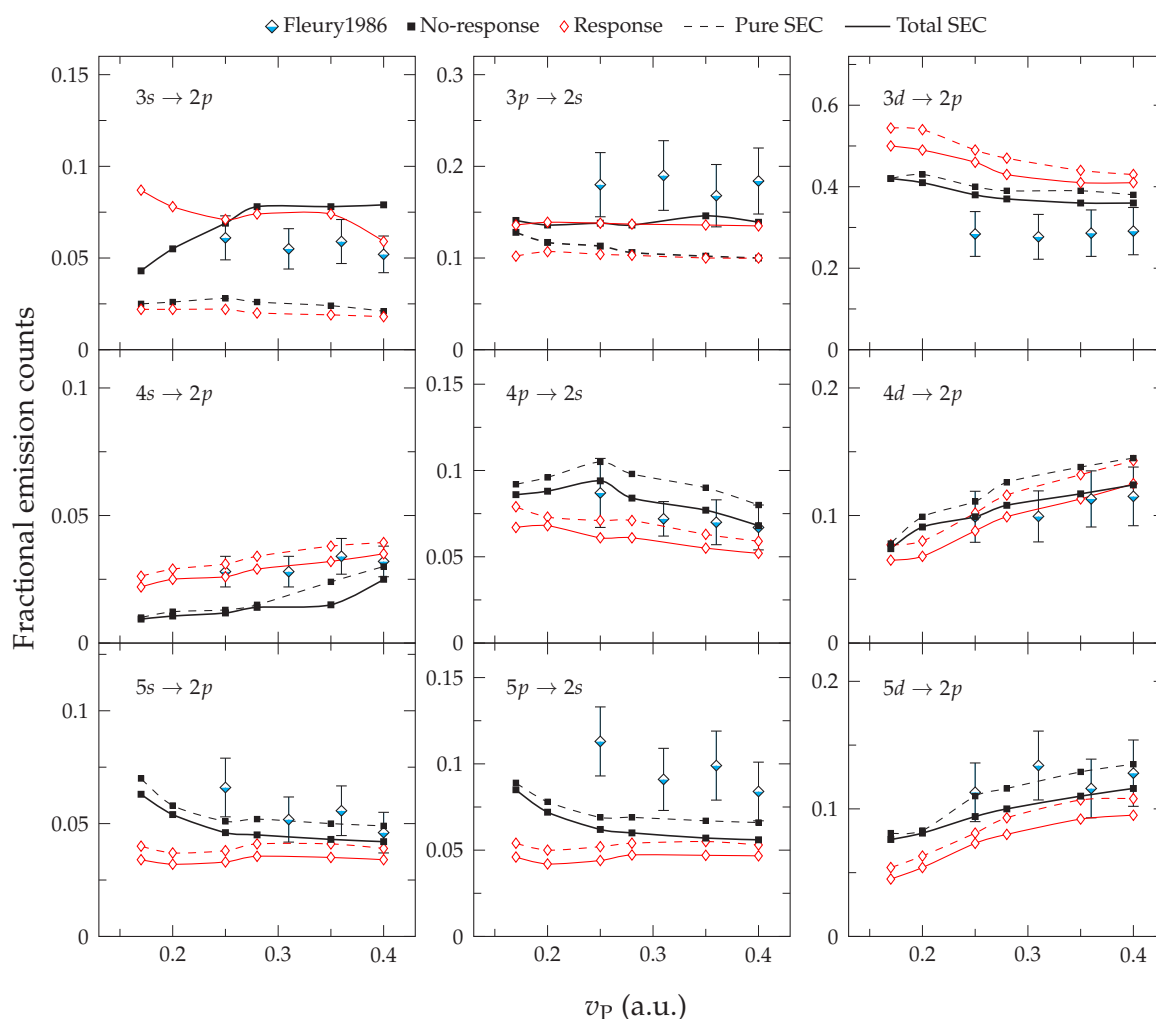**Figure 4.** Fractions of line emissions with respect to impact speed from charge-exchange Ne^{8+}–H_2 collisions. Experiment: Fleury et al. [16]. Theory: present work separated in pure SEC (dashed lines) and total SEC (solid lines).

The comparison of emission counts shows that there is reasonable agreement between the theoretical and the experimental results [16]. One should first note that the present results produced by the two TC-BGM variants are mostly similar but can differ by more than 40% for $v_P \leq 0.25$ a.u. Including contributions from ADC leads to noticeable changes in the $3l \rightarrow 2l'$ transition counts and brings the calculations to closer agreement with the experiments. This is an indication that the counts reported by Fleury et al. [16] likely contain contributions from ADC. Although the inclusion of ADC also affects the fractions of all other transitions, the changes in those counts are not significant. Overall,

the results produced from the present IEM TC-BGM calculations are in satisfactory agreement with the experimental results.

4. Conclusions

Charge exchange in slow Ne^{8+} collisions with He and H_2 and the subsequent radiative emissions were investigated based on the IEM framework, where single-particle probabilities were calculated using the TC-BGM. Model potentials were employed to represent the Ne^{8+} ion and the H_2 target in the collision calculations, while He was represented on the exact-exchange level.

Cross sections for pure SEC obtained from the present calculations generally show good agreement with the available experimental and theoretical data. Good agreement with previous results is also found for the total SEC cross sections when ADC is taken into account, which demonstrates the applicability of the IEM and effective potentials to describe double-capture in these collision systems.

Similarly, the present *nl* partial cross sections are mostly consistent with the available experimental data. Discrepancies found for some states may be due to problems associated with anisotropy effects in the measurements. Although this affected certain spectral line-emission counts, overall, the range of results produced from the present calculations is in reasonable agreement with the available line-emission measurements. It would be of interest to utilize modern experimental techniques, such as cold-target recoil-ion momentum spectroscopy [57], to revisit these collision systems to help resolve these discrepancies.

References

1. Lisse, C.M.; Dennerl, K.; Englhauser, J.; Harden, M.; Marshall, F.E.; Mumma, M.J.; Petre, R.; Pye, J.P.; Ricketts, M.J.; Schmitt, J.; et al. Discovery of X-ray and Extreme Ultraviolet Emission from Comet C/Hyakutake 1996 B2. *Science* **1996**, *274*, 205. [CrossRef]
2. Beiersdorfer, P.; Olson, R.E.; Brown, G.V.; Chen, H.; Harris, C.L.; Neill, P.A.; Schweikhard, L.; Utter, S.B.; Widmann, K. X-Ray Emission Following Low-Energy Charge Exchange Collisions of Highly Charged Ions. *Phys. Rev. Lett.* **2000**, *85*, 5090. [CrossRef] [PubMed]
3. Cravens, T.E. X-ray Emission from Comets. *Science* **2002**, *296*, 1042–1045. [CrossRef] [PubMed]
4. Cravens, T.E. Heliospheric X-ray Emission Associated with Charge Transfer of the Solar Wind with Interstellar Neutrals. *Astrophys. J.* **2000**, *532*, L153. [CrossRef] [PubMed]
5. Koutroumpa, D.; Lallement, R.; Kharchenko, V.; Dalgarno, A.; Pepino, R.; Izmodenov, V.; Quémerais, E. Charge-transfer induced EUV and soft X-ray emissions in the heliosphere. *Astron. Astrophys.* **2006**, *460*, 289–300. [CrossRef]
6. Krasnopolsky, V.A. CXO X-ray spectroscopy of comets and abundances of heavy ions in the solar wind. *Icarus* **2015**, *247*, 95–102. [CrossRef]
7. Cumbee, R.S.; Henley, D.B.; Stancil, P.C.; Shelton, R.L.; Nolte, J.L.; Wu, Y.; Schultz, D.R. Can charge exchange explain anomalous soft x-ray emission in the Cygnus loop? *Astrophys. J. Lett.* **2014**, *787*, L31. [CrossRef]
8. Cumbee, R.S.; Mullen, P.D.; Lyons, D.; Shelton, R.L.; Fogle, M.; Schultz, D.R.; Stancil, P.C. Charge Exchange X-Ray Emission due to Highly Charged Ion Collisions with H, He, and H_2 : Line Ratios for Heliospheric and Interstellar Applications. *Astrophys. J.* **2017**, *852*, 7. [CrossRef]
9. Ali, R.; Neill, P.A.; Beiersdorfer, P.; Harris, C.L.; Schultz, D.R.; Stancil, P.C. Critical Test of Simulations of Charge-Exchange-Induced X-ray Emission in the Solar System. *Astrophys. J. Lett.* **2010**, *716*, L95. [CrossRef]

10. Wu, Y.; Stancil, P.C.; Schultz, D.R.; Hui, Y.; Liebermann, H.P.; Buenker, R.J. Theoretical investigation of total and state-dependent charge exchange in O^{6+} collisions with atomic hydrogen. *J. Phys. B* **2012**, *45*, 235201. [CrossRef]

11. Machacek, J.R.; Mahapatra, D.P.; Schultz, D.R.; Ralchenko, Y.; Moradmand, A.; El Ghazaly, M.O.A.; Chutjian, A. Solar-Wind Ion-Driven X-ray Emission from Cometary and Planetary Atmospheres: Measurements and Theoretical Predictions of Charge-Exchange Cross-Sections and Emission Spectra for O^{6+} + H_2O, CO, CO_2, CH_4, N_2, NO, N_2O, and Ar. *Astrophys. J.* **2015**, *809*, 75. [CrossRef]

12. Ali, R.; Beiersdorfer, P.; Harris, C.L.; Neill, P.A. Charge-exchange x-ray spectra: Evidence for significant contributions from radiative decays of doubly excited states. *Phys. Rev. A* **2016**, *93*, 012711. [CrossRef]

13. Bonnet, J.J.; Fleury, A.; Bonnefoy, M.; Politis, M.F.; Chassevent, M.; Bliman, S.; Dousson, S.; Hitz, D. Electron capture into different (nl) states in slow collisions of Ne^{8+} projectiles on He and H_2 targets. *J. Phys. B* **1985**, *18*, L23–L27. [CrossRef]

14. Druetta, M.; Mayo, M.; Bliman, S.; Martin, S.; Hitz, D.; Dousson, S.; Desesquelles, J. Etude spectroscopique de la collision d'échange de charge entre Ne^{8+} et He. *J. Physique Lett.* **1985**, *46*, 869–873. [CrossRef]

15. Beijers, J.P.M.; Hoekstra, R.; Morgenstern, R. State-selective charge transfer between He-like ions and He. *Phys. Rev. A* **1994**, *49*, 363–373. [CrossRef] [PubMed]

16. Fleury, A.; Debernardi, J.; Bonnefoy, M.; Bliman, S.; Bonnet, J.J.; Chassevent, M. A simple soft X-ray ($1 < \lambda < 11$ nm) spectrometer for relative line intensity measurements in charge exchange studies. *Nucl. Instrum. Methods Phys. Res. Sect. B* **1986**, *14*, 353–359.

17. Harel, C.; Jouin, H. Double capture into autoionizing states in I^{q+} -He collisions at low impact energies. *J. Phys. B* **1992**, *25*, 221–237. [CrossRef]

18. Politis, M.F.; Jouin, H.; Bonnefoy, M.; Bonnet, J.J.; Chassevent, M.; Fleury, A.; Bliman, S.; Harel, C. Relative (n, l) populations following electron capture by low energy N^{7+}, O^{8+} and Ne^{8+} ions from two-electron targets (H_2, He). *J. Phys. B* **1987**, *20*, 2267–2279. [CrossRef]

19. McCammon, D.; Barger, K.; Brandl, D.E.; Brekosky, R.P.; Crowder, S.G.; Gygax, J.D.; Kelley, R.L.; Kilbourne, C.A.; Lindeman, M.A.; Porter, F.S.; et al. The X-ray Quantum Calorimeter Sounding Rocket Experiment: Improvements for the Next Flight. *J. Low Temp. Phys.* **2008**, *151*, 715–720. [CrossRef]

20. Zhang, R.T.; Wulf, D.; Jaeckel, F.; McCammon, D.; Seely, D.G.; Andrianarijaona, V.M.; Cumbee, R.S.; Stancil, P.C.; Havener, C.C. High-resolution charge exchange X-ray emission at solar wind velocities. **2018**, submitted.

21. Zhang, R.T. (Oak Ridge National Laboratory, Oak Ridge, TN, USA). Personal communication, 2018.

22. McGuire, J.H.; Weaver, L. Independent electron approximation for atomic scattering by heavy particles. *Phys. Rev. A* **1977**, *16*, 41. [CrossRef]

23. Jain, A.; Lin, C.D.; Fritsch, W. Electron capture in C^{6+} + He and O^{8+} + He collisions at intermediate energies in the atomic-orbital-expansion method. *Phys. Rev. A* **1986**, *34*, 3676–3683. [CrossRef]

24. Shingal, R.; Lin, C.D. Calculations of two-electron transition cross sections between fully stripped ions and helium atoms. *J. Phys. B* **1991**, *24*, 251–264. [CrossRef]

25. Chen, Z.; Shingal, R.; Lin, C.D. State-selective double capture in collisions of bare ions with helium atoms at low energies. I. Total cross sections. *J. Phys. B* **1991**, *24*, 4215–4230. [CrossRef]

26. Chen, Z.; Lin, C.D. Double electron capture and the angular distribution of ejected electrons in Ne^{8+}-He collisions. *Phys. Rev. A* **1993**, *48*, 1298–1307. [CrossRef] [PubMed]

27. Errea, L.F.; Gorfinkiel, J.D.; Harel, C.; Jouin, H.; Macías, A.; Méndez, L.; Pons, B.; Riera, A. Model potential treatment of C^{4+}+H_2 collisions at low impact energies. *J. Phys. B* **2000**, *33*, 3107. [CrossRef]

28. Zapukhlyak, M.; Kirchner, T.; Lüdde, H.J.; Knoop, S.; Morgenstern, R.; Hoekstra, R. Inner- and outer-shell electron dynamics in proton collisions with sodium atoms. *J. Phys. B* **2005**, *38*, 2353. [CrossRef]

29. Zapukhlyak, M.; Kirchner, T.; Hasan, A.; Tooke, B.; Schulz, M. Projectile angular-differential cross sections for transfer and transfer excitation in proton collisions with helium. *Phys. Rev. A* **2008**, *77*, 012720. [CrossRef]

30. Knoop, S.; Fischer, D.; Xue, Y.; Zapukhlyak, M.; Osborne, C.J.; Ergler, T.; Ferger, T.; Braun, J.; Brenner, G.; Bruhns, H.; et al. Single-electron capture in keV Ar $^{15+...18+}$+He collisions. *J. Phys. B* **2008**, *41*, 195203. [CrossRef]

31. Röhrbein, D.; Kirchner, T.; Fritzsche, S. Role of cascade and Auger effects in the enhanced population of the $C^{3+}(1s2s2p\ ^4P)$ states following single-electron capture in $C^{4+}(1s2s\ ^3S)$-He collisions. *Phys. Rev. A* **2010**, *81*, 042701. [CrossRef]

32. Schenk, G.; Kirchner, T. Multiple ionization of neon atoms in collisions with bare and dressed ions: A mean-field description considering target response. *Phys. Rev. A* **2015**, *91*, 052712. [CrossRef]

33. Salehzadeh, A.; Kirchner, T. Strong multiple-capture effect in slow Ar $^{17+}$ -Ar collisions: A quantum mechanical analysis. *J. Phys. B* **2013**, *46*, 025201. [CrossRef]

34. Leung, A.C.K.; Kirchner, T. Independent-electron analysis of the x-ray spectra from single-electron capture in Ne^{10+} collisions with He, Ne, and Ar atoms. *Phys. Rev. A* **2015**, *92*, 032712. [CrossRef]

35. Leung, A.C.K.; Kirchner, T. Analysis of x-ray emission spectra in charge-exchange collisions of C^{6+} with He and H$_2$. *Phys. Rev. A* **2016**, *93*, 052710. [CrossRef]

36. Leung, A.C.K.; Kirchner, T. Lyman line ratios in charge-exchange collisions of C^{6+} and O^{8+} ions with hydrogen and krypton atoms. *Phys. Rev. A* **2018**, *97*, 062705. [CrossRef]

37. Harel, C.; Jouin, H. Electron capture by slow multicharged ions: core effect on final l-distributions. *J. Phys. B* **1988**, *21*, 859–883. [CrossRef]

38. Engel, E.; Vosko, S.H. Accurate optimized-potential-model solutions for spherical spin-polarized atoms: Evidence for limitations of the exchange-only local spin-density and generalized-gradient approximations. *Phys. Rev. A* **1993**, *47*, 2800. [CrossRef] [PubMed]

39. Kirchner, T.; Horbatsch, M.; Lüdde, H.J.; Dreizler, R.M. Time-dependent screening effects in ion-atom collisions with many active electrons. *Phys. Rev. A* **2000**, *62*, 042704. [CrossRef]

40. Kirchner, T.; Horbatsch, M.; Lüdde, H.J. Time-dependent independent-particle model calculation of multiple capture and ionization processes in *p*-Ar, *p̄*-Ar, and He^{2+}-Ar collisions. *Phys. Rev. A* **2002**, *66*, 052719. [CrossRef]

41. Chung, H.K.; Braams, B.J.; Bartschat, K.; Csaszar, A.G.; Drake, G.W.F.; Kirchner, T.; Kokoouline, V.; Tennyson, J. Uncertainty Estimates for Theoretical Atomic and Molecular Data. *J. Phys. D* **2016**, *49*, 363002. [CrossRef]

42. Horbatsch, M. A semiclassical time-dependent Hartree model calculation of capture and multiple ionization in heavy ion-Ar collisions. *Phys. Lett. A* **1994**, *187*, 185. [CrossRef]

43. Kirchner, T.; Lüdde, H.J.; Horbatsch, M.; Dreizler, R.M. Quantum-mechanical description of ionization, capture, and excitation in proton collisions with atomic oxygen. *Phys. Rev. A* **2000**, *61*, 052710. [CrossRef]

44. Curtis, L.J. A Diagrammatic Mnemonic for Calculation of Cascading Level Populations. *Am. J. Phys.* **1968**, *36*, 1123–1125. [CrossRef]

45. Younger, S.M.; Wiese, W.L. Theoretical simulation of beam-foil decay curves for resonance transitions of heavy ions. *Phys. Rev. A* **1978**, *17*, 1944. [CrossRef]

46. Fritzsche, S. The RATIP program for relativistic calculations of atomic transition, ionization and recombination properties. *Comput. Phys. Commun.* **2012**, *183*, 1525–1559. [CrossRef]

47. Mack, M.; Nijland, J.H.; Straten, P.V.D.; Niehaus, A.; Morgenstern, R. Correlation in double electron capture in collisions of fully stripped ions on He and H$_2$. *Phys. Rev. A* **1989**, *39*, 3846. [CrossRef]

48. Iwai, T.; Kaneko, Y.; Kimura, M.; Kobayashi, N.; Ohtani, S.; Okuno, K.; Takagi, S.; Tawara, H.; Tsurubuchi, S. Cross sections for one-electron capture by highly stripped ions of B, C, N, O, F, Ne, and S from He below 1 keV/amu. *Phys. Rev. A* **1982**, *26*, 105–115. [CrossRef]

49. Panov, M.N.; Basalaev, A.A.; Lozhkin, K.O. Interaction of Fully Stripped, Hydrogenlike and Heliumlike C, N, O, Ne and Ar Ions with H and He Atoms and H$_2$ Molecules. *Phys. Scr.* **1983**, *T3*, 124–130. [CrossRef]

50. Boudjema, M.; Cornille, M.; Dubau, J.; Moretto-Capelle, P.; Bordenave-Montesquieu, A.; Benoit-Cattin, P.; Gleizes, A. Investigation of double capture in Ne^{8+}+ He, H$_2$, by electron spectroscopy at 80 keV. II. Experimental results. *J. Phys. B* **1991**, *24*, 1713–1737. [CrossRef]

51. Dunseath, K.M.; Crothers, D.S.F. Transfer and ionization processes during the collision of fast H$^+$, He^{2+} nuclei with helium. *J. Phys. B* **1991**, *24*, 5003. [CrossRef]

52. Roncin, P.; Barat, M.; Laurent, H. Differential Cross-Sections for One- and Two-Electron Capture by Highly Charged Ions (N^{7+}, O^{7+}, O^{8+}, Ne^{7+}, Ne^{8+}) at Low keV Energies. *Europhys. Lett.* **1986**, *2*, 371–377. [CrossRef]

53. Barat, M.; Gaboriaud, M.N.; Guillemot, L.; Roncin, P.; Laurent, H.; Andriamonje, S. Coincident energy gain spectroscopy of electron capture in multiply charged ions colliding with He, H$_2$ and heavy rare-gas targets. *J. Phys. B* **1987**, *20*, 5771–5783. [CrossRef]

54. Mack, M. Electron spectroscopy in collisions with multiply charged ions. *Nucl. Instrum. Methods Phys. Res. Sect. B* **1987**, *23*, 74–85. [CrossRef]

55. Bordenave-Montesquieu, A.; Boudjema, M.; Benoit-Cattin, P.; Gleizes, A.; Moretto-Capelle, P. *Q*-Dependence of the Double Capture Cross Sections Measured by Electron Spectroscopy at 10 $q$keV ($q = 4 - 8$). Comparison with other Experimental Data. *J. Physique Colloques* **1989**, *50*, C1-305–C1-312. [CrossRef]

56. Janev, R.K.; Winter, H. State-selective electron capture in atom-highly charged ion collisions. *Phys. Rep.* **1985**, *117*, 265–387. [CrossRef]

57. Ullrich, J.; Moshammer, R.; Dorn, A.; Dörner, R.; Schmidt, L.P.H.; Schmidt-Böcking, H. Recoil-ion and electron momentum spectroscopy: Reaction-microscopes. *Reports Prog. Phys.* **2003**, *66*, 1463–1545. [CrossRef]